ORNL/TM-2023/2997

A Systematic Approach for Estimating High-Altitude Electromagnetic Pulse Coupling onto Power Generation Facility Equipment

DaHan Liao
Yilu Liu
Lawrence C. Markel
Benjamin W. McConnell
David P. Mignardot
Brian R. Poole
Lisa Wang

August 2023

OAK RIDGE National Laboratory

ORNL IS MANAGED BY UT-BATTELLE LLC FOR THE US DEPARTMENT OF ENERGY

ORNL/TM-2023/2997

Energy Science and Technology Directorate
Electrification and Energy Infrastructures Division

A SYSTEMATIC APPROACH FOR ESTIMATING HIGH-ALTITUDE ELECTROMAGNETIC PULSE COUPLING ONTO POWER GENERATION FACILITY EQUIPMENT

DaHan Liao
Yilu Liu
Lawrence C. Markel
Benjamin W. McConnell
David P. Mignardot
Brian R. Poole
Lisa Wang

August 2023

Prepared by
OAK RIDGE NATIONAL LABORATORY
Oak Ridge, TN 37831
managed by
UT-Battelle LLC
for the
US DEPARTMENT OF ENERGY
under contract DE-AC05-00OR22725

CONTENTS

LIST OF FIGURES

LIST OF TABLES

ABBREVIATIONS

BLT	Baum–Liu–Tesche
HEMP	high-altitude electromagnetic pulse
MoM	method-of-moments
ORNL	Oak Ridge National Laboratory
PLC	programmable logic controller
PMU	phasor measurement unit

ABSTRACT

A systematic approach is presented to evaluate the effects of high-altitude electromagnetic pulse (HEMP) signals on the equipment located inside a power generation facility. The approach uses a combination of practical measurement and simulation efforts to characterize the radio wave propagation behavior and the device immunity profile. Of particular interest in this work was estimating the vulnerability level of equipment that is connected to long cables. As an example application, a detailed study was conducted for one common class of facility equipment, and its frequency- and time-domain HEMP coupling properties were investigated as a function of terminal loading condition and cable attachment configuration. Overall, the proposed method can be generalized and applied to other electronic components and systems found in the facility environment.

1. INTRODUCTION

As a response to increased US government and commercial interest in energy infrastructure protection against electromagnetic threats, an investigation was conducted on the effects of fast, high-intensity transients on the equipment located inside power generation facilities. The waveform of primary concern in this work was the early-time (E1) component that is produced by a nuclear explosion detonated high in the atmosphere; this so-called high-altitude electromagnetic pulse (HEMP) event has the potential to catastrophically affect the electrical infrastructure over a very wide area [1; 2; 3; 4; 5]. Although a building's physical structure can provide a certain level of shielding against external radiative electromagnetic attacks, the shielding effectiveness can vary drastically depending on the construction material, frequency, and location within the facility; a HEMP signal coupled into the facility, even if weakened, can still carry sufficient energy to cause significant disruption or damage, especially to low-voltage, semiconductor-based electronic systems. Of particular concern is when such equipment is attached to long cables or wires because these conductors tend to act like antennas in picking up electromagnetic energy while also serving as conduits for propagating energy to any connected component (Figure 1). A systematic approach is proposed in this report for analyzing E1 HEMP coupling onto the ports of facility equipment. The results can subsequently be used to assess system vulnerability and provide guidance in developing mitigation measures.

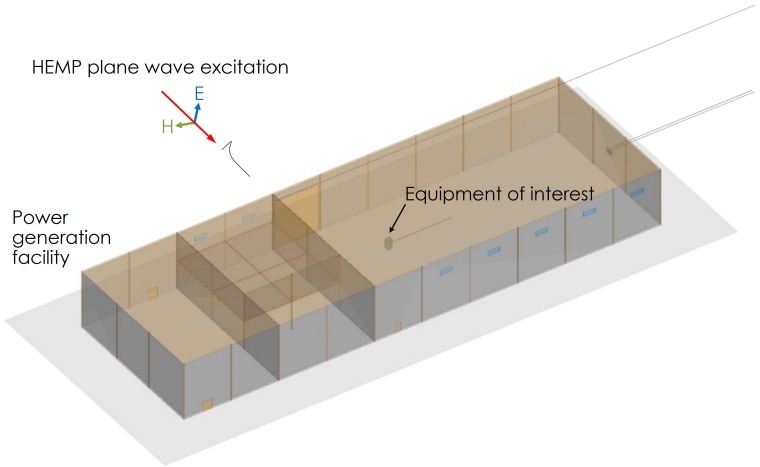

Figure 1. Coupling of HEMP signal onto facility equipment.

2. ANALYSIS FRAMEWORK

The technique for calculating the induced voltages and currents on the equipment ports followed a four-step procedure that combined measurement and simulation efforts (Figure 2). A brief outline of each step is presented in the following sections. As mentioned, the excitation waveform is E1 HEMP, the time- and frequency-domain characteristics for which are outlined in [6].

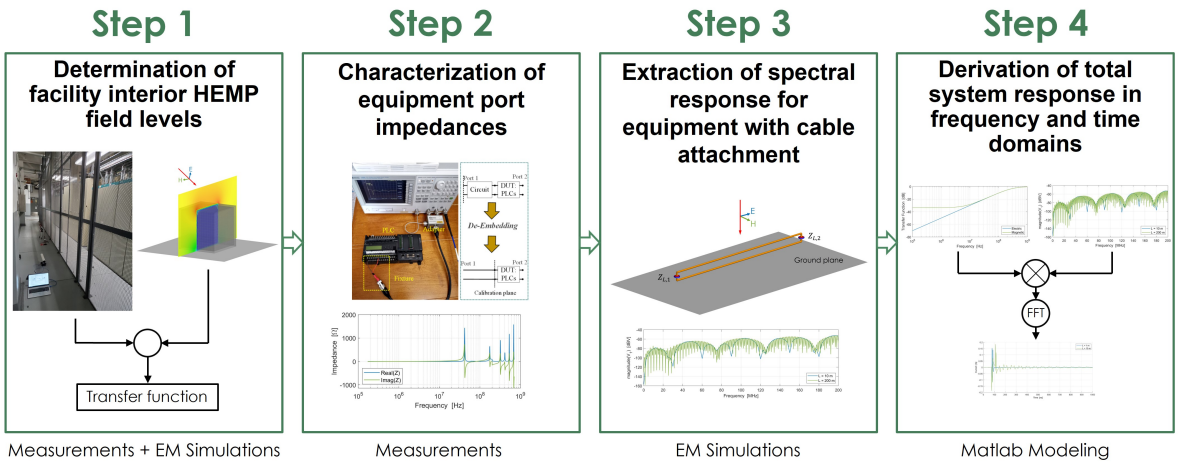

Figure 2. Estimation of HEMP-induced voltage and current on equipment: overview of methods and techniques.

2.1 STEP 1: DETERMINATION OF FACILITY INTERIOR HEMP FIELD LEVELS

Deriving the complete propagation characteristics of a full-scale power generation facility solely by electromagnetic simulations is intractable because of computational resource constraints. Therefore, a semiempirical approach was undertaken that consists of complementing building shielding–effectiveness measurements with wave simulation results for simple canonical models [6]. Onsite measurements of ambient signals—such as those from cellular, broadcast radio, and television transmitters—were first obtained [7; 8]. By computing the ratio of exterior and interior field levels, shielding effectiveness values were obtained at locations of interest such as the control room, generator room, cable spreading room, etc. Although the reliance on ambient illuminators may have limited the number of frequency points for which the coupling could be calculated empirically, this passive approach was more practical compared with an active one that requires the irradiation of the plant with an on-site transmitter because there are often operational and regulatory restrictions on the transmission of high-power signals, especially over a wide frequency band. To understand the propagation characteristics over the entire E1 HEMP frequency band, electromagnetic simulations of small-scale, canonical building structures were also performed as functions of frequency, construction material, signal angle, wave polarization, and ground plane properties; essentially, the simulation data complemented the measurement data by filling in frequency gaps where no ambient sources may have been present [6]. As an example, the electric and magnetic transfer functions for a facility control room are shown in Figure 3, and the corresponding E1-induced signals are shown in Figure 4.

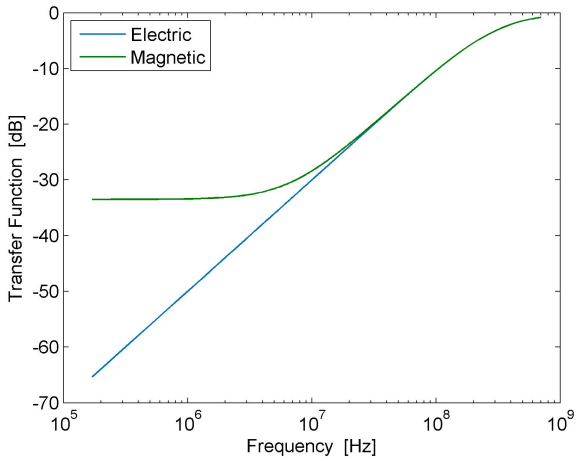

Figure 3. Transfer functions for the facility control room as deduced from on-site shielding effectiveness measurements and electromagnetic simulations.

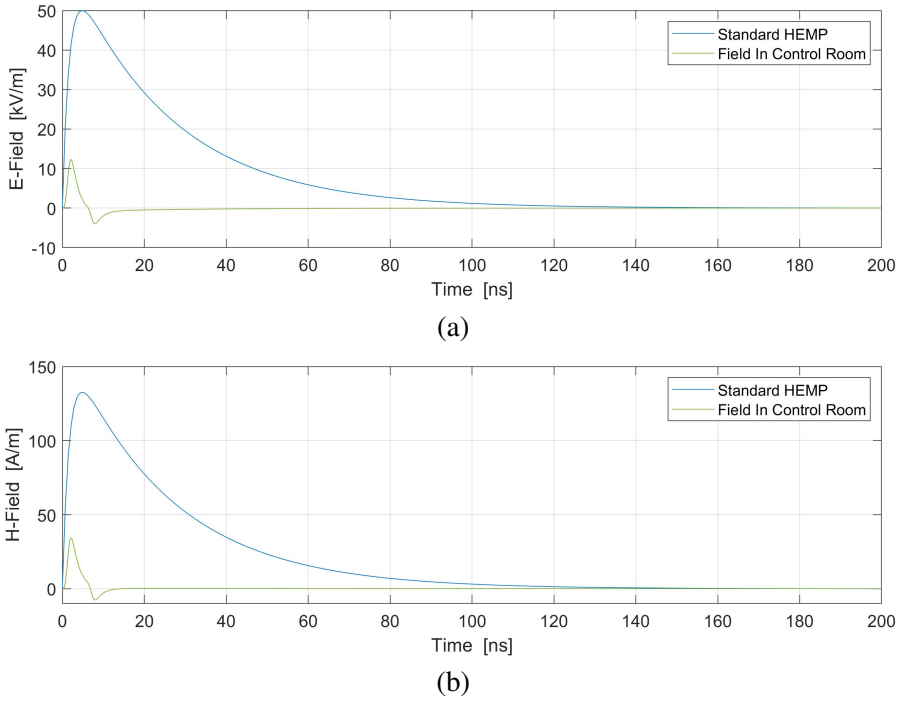

Figure 4. Interior E1 fields for the facility control room (averaged): (a) electric and (b) magnetic.

2.2 STEP 2: CHARACTERIZATION OF EQUIPMENT PORT IMPEDANCES

Terminal loading conditions are an important factor in determining the amount of electromagnetic energy that cables and wires can pick up. Therefore, to evaluate the HEMP signal that eventually propagates into the equipment, the impedances seen at all the device ports must be characterized. In this study, port

impedances were verified experimentally in the laboratory for three programmable logic controllers (PLCs) and one phasor measurement unit (PMU) as described in Qiu et al. [9] and Zhang et al. [10] (Figure 5), which propose a measurement scheme based on the use of three different instruments—namely, an LCR meter, an impedance analyzer, and a vector network analyzer—with each covering a separate frequency sub-band. To obtain the impedances over the complete E1 HEMP frequency range, the three measured data sets were integrated using interpolation and data-averaging techniques. Note that a special procedure must be developed to eliminate the influence of the measurement fixture; specifically, a nonuniform transmission line model was established to approximate and subsequently de-embed the impedance effects of the fixture. Because each device can have a different circuit layout, the measurement data (Figures 6 and 7) show that the port impedances can vary significantly depending on the device model and the manufacturer. As outlined in Qiu et al. [9] and Zhang et al. [10], a pulse current injection method is also proposed to simulate how the PLCs and the PMU would react to fast transients caused by a HEMP event; however, results from this method assume that the excitation is provided by a standard waveform without building attenuation and cable coupling effects.

PLC 1:
Allen Bradley 1766-L326BWA

PLC 2:
BX-DM1-36ER-D

PLC 3:
AutomationDirect DL06 Micro

PMU:
Powerside PQube 3

Figure 5. The three PLCs and one PMU studied in this work.

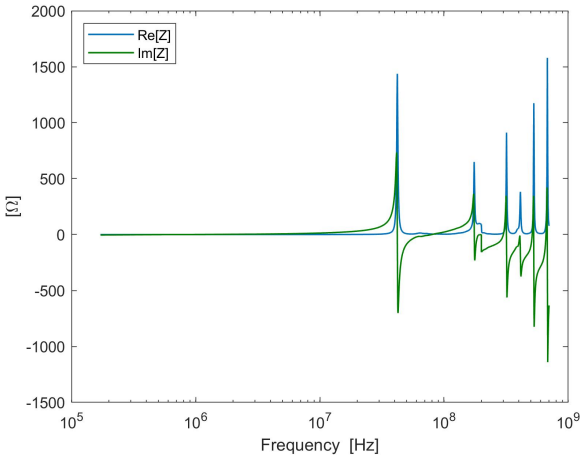

(a)

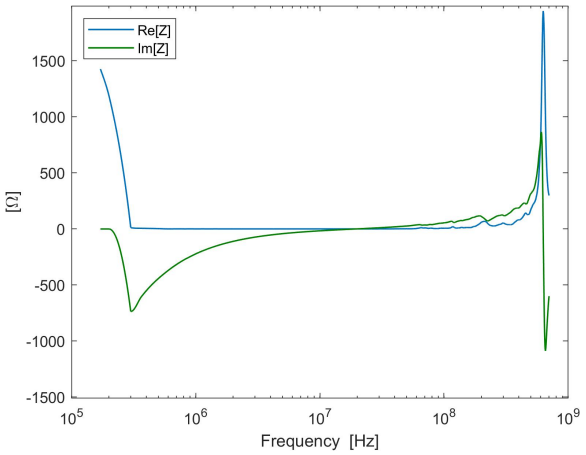

(b)

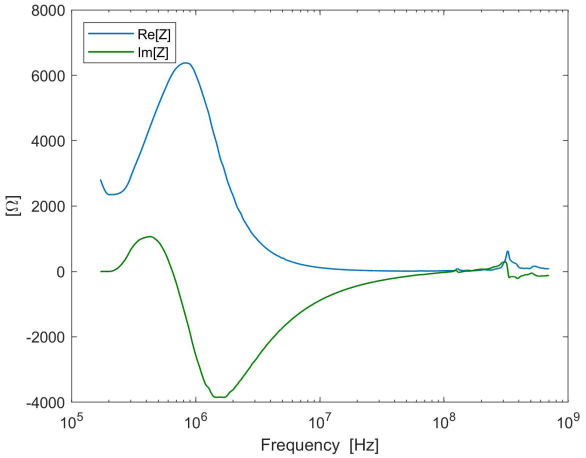

(c)

Figure 6. Port impedances for the three PLCs: (a) PLC 1, (b) PLC 2, and (c) PLC 3. Re[Z] and Im[Z] denote the real and imaginary parts of the impedance, respectively.

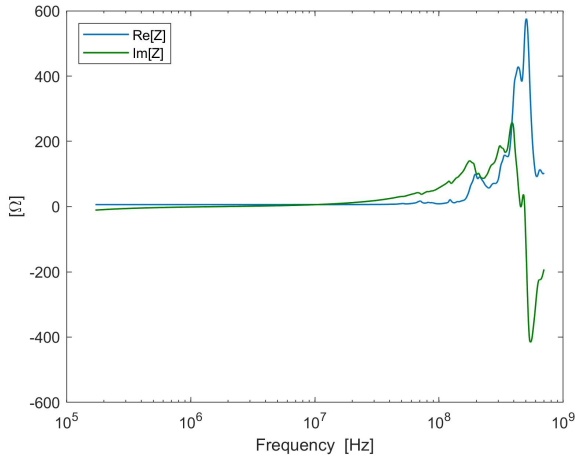

(a)

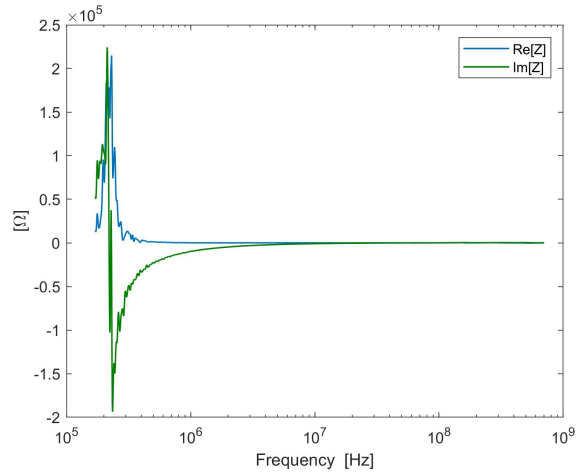

(b)

Figure 7. Port impedances for the PMU: (a) wire-wire and (b) wire-ground.

2.3 STEP 3: EXTRACTION OF SPECTRAL RESPONSE FOR EQUIPMENT WITH CABLE ATTACHMENT

Next, frequency-domain full-wave simulations were performed to characterize the spectral response of cables loaded with the measured port impedances from the previous step; therefore, in effect, the equipment appeared at the cable terminals (in the electromagnetic models) only as frequency-dependent loads. The cable geometries were created and simulated in a method-of-moments (MoM) solver as implemented by a commercial software package [11]. For each model, a cable of length L was situated at a height h above a perfectly conducting ground plane; the terminal voltage and current responses were characterized as functions of frequency, cable length, and height for each device, with the excitation provided by a plane wave of unity amplitude. Because the exact polarization of the wave irradiating the equipment and cable attachment in a real facility setting was not known, a worst-case scenario was assumed to simplify the analysis; that is, for example, in the case of a two-wire model, the incident electric field vector was set to be

parallel to the geometrical plane containing the wires to establish maximum coupling (Figure 8).

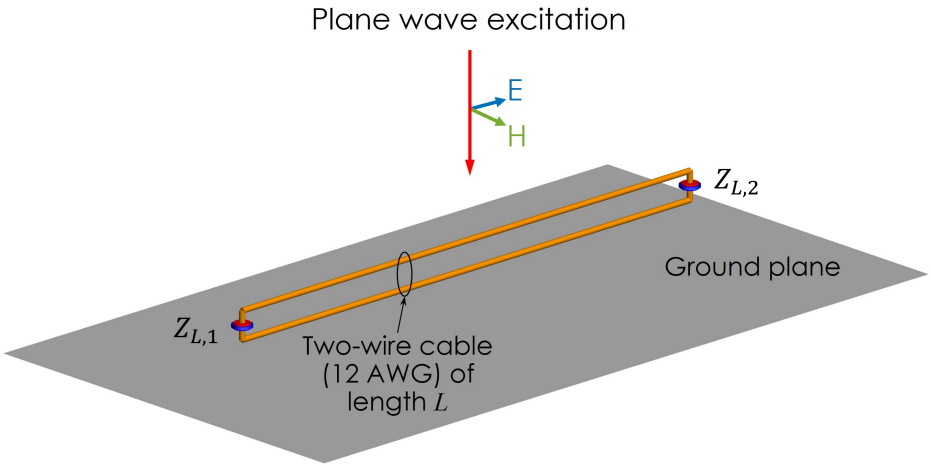

Figure 8. Electromagnetic simulation model for a two-wire cable: $Z_{L,1}$ is the terminal impedance matched to the cable characteristic impedance, and $Z_{L,2}$ is the equipment load impedance as determined from measurements. The cable is located at height h above the ground plane.

Although this study mainly focuses on applying a full-wave solver to determine the coupling response of the cable, an alternative method, the Baum–Liu–Tesche (BLT) solution [12; 13; 14; 15], was also explored for instructive purposes to understand the numerical results. The BLT solution is based on deriving propagation relationships for the incident and reflected voltages and wave fields traveling in propagation tubes that lie along transmission lines or in space. Referring to the setup in Figure 9, the voltages and waves can be shown to satisfy the following system of equations:

$$v_{1,1}^{ref} = e^{\gamma L} v_{1,2}^{inc} - F_1 K_1(r_o) a_3 E_{2,3}^{ref} - F_1 K_1(r_1) S_1 \tag{1}$$

$$v_{1,2}^{ref} = e^{\gamma L} v_{1,1}^{inc} - F_2 K_1(r_o) a_3 E_{2,3}^{ref} - F_2 K_1(r_1) S_1 \tag{2}$$

$$v_{1,1}^{ref} = v_{1,1}^{inc} \Gamma_1 \tag{3}$$

$$v_{1,2}^{ref} = v_{1,2}^{inc} \Gamma_2 \tag{4}$$

$$E_{2,3}^{inc} = a_4 E_{2,4}^{ref} K_2(r_o) + \frac{jk_o Z_o}{2\pi Z_c} K_1(r_o) \left(F_1 v_{1,1}^{inc} + F_2 v_{1,2}^{inc} \right) + K_3(r_2) S_2 \tag{5}$$

$$E_{2,4}^{inc} = a_3 E_{2,3}^{ref} K_2(r_o) + K_2(r_1) S_1 \tag{6}$$

$$a_3 E_{2,3}^{ref} = \sigma_3 E_{2,3}^{inc} \tag{7}$$

$$a_4 E_{2,4}^{ref} = \sigma_4 E_{2,4}^{inc} \tag{8}$$

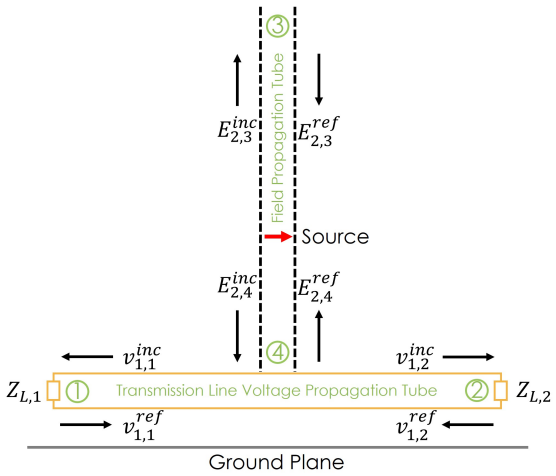

Figure 9. Definitions for the BLT solution.

Eqs. (1)–(4) are applied to the field propagation tube, and Eqs. (5)–(8) are applied to the transmission line voltage propagation tube. In solving for $v^{inc}_{1,1}$, $v^{ref}_{1,1}$, $v^{inc}_{1,2}$, $v^{ref}_{1,2}$, $E^{inc}_{2,3}$, $E^{inc}_{2,4}$, $a_3E^{ref}_{2,3}$, and $a_4E^{ref}_{2,4}$, the following definitions are needed [16; 17]: γ is the propagation constant of the transmission line; $F_{1,2}$ are coupling functions; $K_{1,2,3}(\cdot)$ are wave expansion factors (including the ground plane image term); $a_{3,4}$ are field-to-voltage conversion factors; $S_{1,2}$ are the source terms; $\Gamma_{1,2}$ are the voltage reflection coefficients; $\sigma_{3,4}$ are the scattering areas/lengths; and Z_c is the transmission line characteristic impedance.

As examples of the coupling response obtained from the BLT technique, Figures 10 and 11 compare the load voltages (amplitude and phase) from the BLT method and from the MoM solution for the model illustrated in Figure 9. The excitation was taken as a point source (i.e., an electric dipole with unity current moment) located at distance $r = 10$ m in Figure 10 and $r = 100$ m in Figure 11. In both cases, $L = 10$ m and $h = 3$ m; the cable wire separation distance was $d = 1$ cm; and $Z_{L,1} = Z_{L,2} = Z_c/2$.

Note that the BLT technique did not give very accurate solutions when the source was close to the transmission line (that is, the incident field over the two wires was not a uniform plane wave), but improved accuracy was observed at a larger distance.

The BLT solution has certain advantages—namely, it is more computationally efficient than full-wave methods and provides an intuitive understanding of the underlying propagation physics. However, it also has the following salient disadvantages: (1) it cannot be easily generalized for implementation in complicated scenarios (e.g., cables with shields, cables penetrating a building, geometries defined by aperture effects), (2) it may require the use of Green's functions that are not known analytically, and (3) it keeps track of only far-field plane wave interactions. Because of these shortcomings, this work mainly relies on full-wave solutions to characterize cable coupling effects.

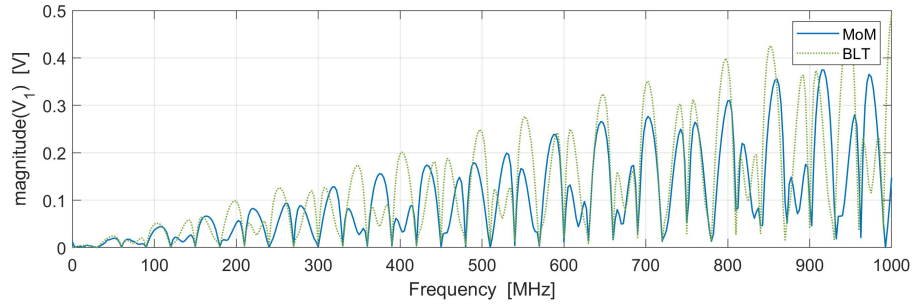

(a)

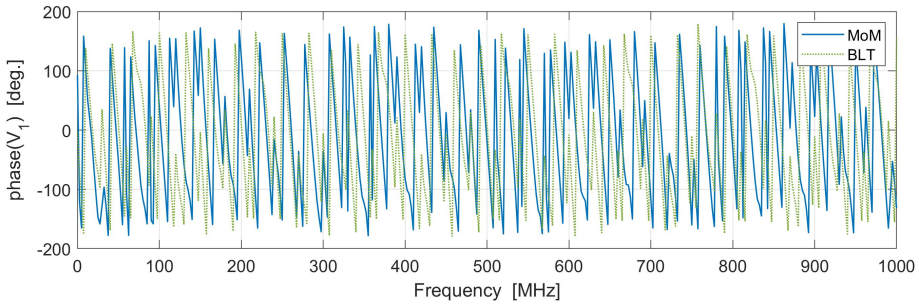

(b)

Figure 10. Load voltage calculated using the BLT solution compared with the MoM solution for r = 10 m: (a) amplitude and (b) phase.

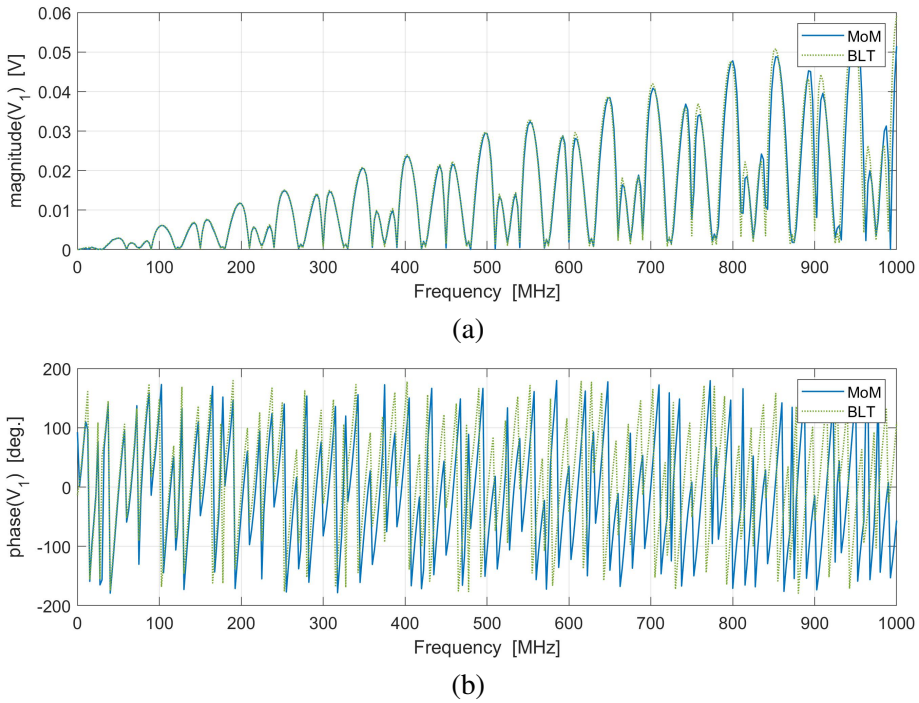

Figure 11. Load voltage calculated using the BLT solution compared with the MoM solution for r = 100 m: (a) amplitude and (b) phase.

2.4 STEP 4: DERIVATION OF TOTAL SYSTEM RESPONSE IN FREQUENCY AND TIME DOMAINS

In the final step of the analysis procedure, the semiempirical building attenuation profile was applied to determine the response of the equipment when placed in a facility environment. Accordingly, for instance, the total (electric or magnetic) system response $S_{E,H}(f)$ at the equipment terminal in the frequency domain is given as

$$S_{E,H}(f) = E_1(f)T_{E,H}(f)C(f), \tag{9}$$

where $E_1(f)$ is the standard E1 HEMP spectrum [6], $T_{E,H}(f)$ is the transfer function deduced in Step 1, and $C(f)$ is the cable plane-wave impulse response from Step 3. The procedure in Step 1 allows only the amplitude component of the transfer function to be measured, but a phase term is also needed to obtain a physical (causal) response. To resolve this inconsistency, the phase term in this work was derived from the equivalent circuits modeling the attenuation profile as presented in Liao et al. [6]. With the frequency-domain responses determined, the time-domain waveforms can be calculated from Eq. (9) with a fast Fourier transform operation. Note that a windowing function may be employed to suppress "ringing" artifacts caused by frequency truncation.

3. RESULTS

The four-step procedure was applied to electromagnetic coupling analysis for three PLCs and one PMU, each with a power cable attachment. The time- and frequency-domain voltage and current responses at the

power ports of the devices are shown in Figures 12–21, with the facility transfer function assumed to be that for the control room [6] (Figure 3). The waveform structures of the responses could be very different depending on the device model because each has its own distinctive impedance characteristics, but in terms of the maximum voltage and current induced, the responses had similar amplitudes (Table 1). Interestingly, although longer cables tend to lead to longer reverberations, increasing the cable length did not always seem to significantly increase coupling, at least for the three cases considered: $L = 1$ m, $L = 10$ m, and $L = 100$ m. In general, the coupled waveforms had faster variations and risetimes than the incident E1 pulse mostly because of the high-pass filtering behavior of the facility transfer function. Also, for the two cable heights studied ($h = 1$ cm and $h = 1$ m), placing the cable closer to the ground plane can lead to higher coupling; this was caused by the higher magnetic field intensity in the vicinity of the ground plane as a consequence of the metallic boundary condition effect. For completeness, the time- and frequency-domain responses of the cable with a matched load at both ends are shown in Figures 22 and 23. Similar analysis as above can be performed for the other ports of the devices—for example, the I/O data and communications ports.

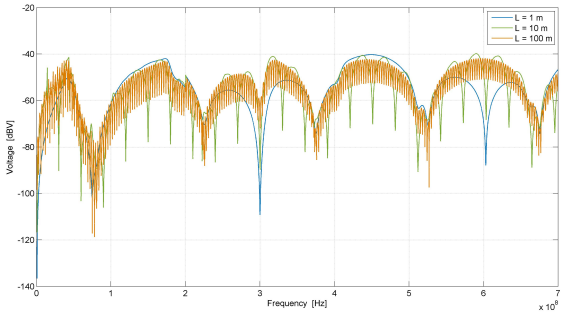

(a)

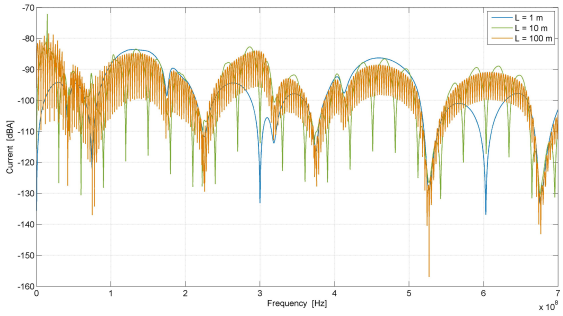

(b)

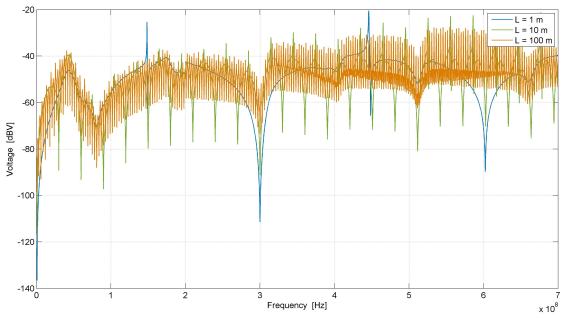

(c)

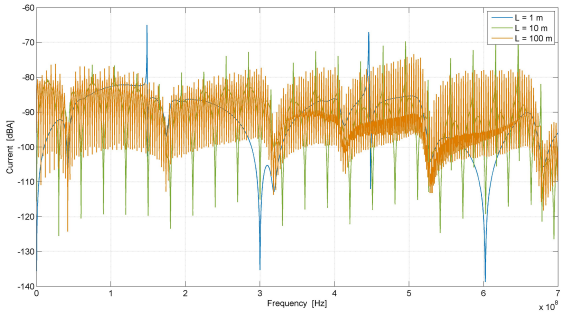

(d)

Figure 12. Induced voltage and current responses on the power port of PLC 1 as a function of frequency for various cable lengths and cable heights: (a) voltage, h = 1 m; (b) current, h = 1 m; (c) voltage, h = 1 cm; and (d) current, h = 1 cm.

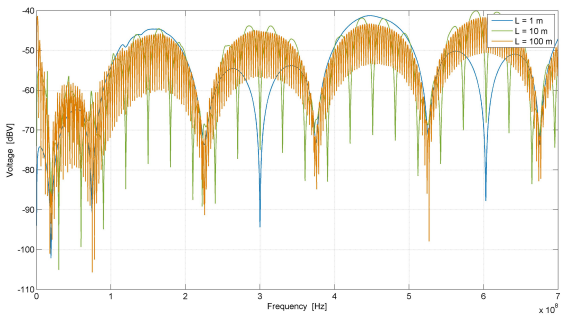

(a)

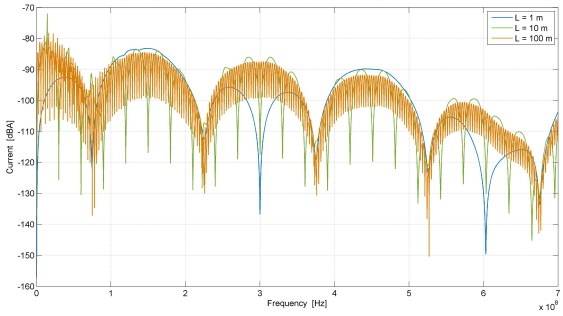

(b)

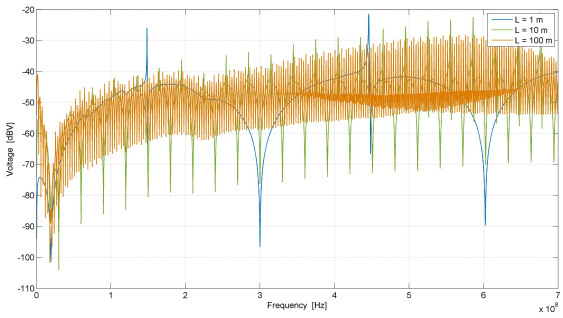

(c)

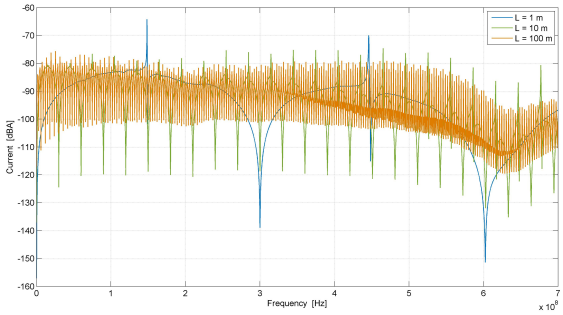

(d)

Figure 13. Induced voltage and current responses on the power port of PLC 2 as a function of frequency for various cable lengths and cable heights: (a) voltage, h = 1 m; (b) current, h = 1 m; (c) voltage, h = 1 cm; and (d) current, h = 1 cm.

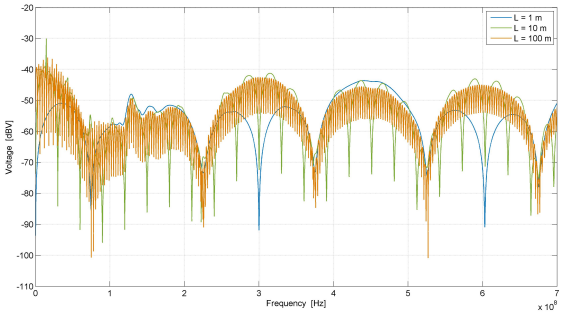

(a)

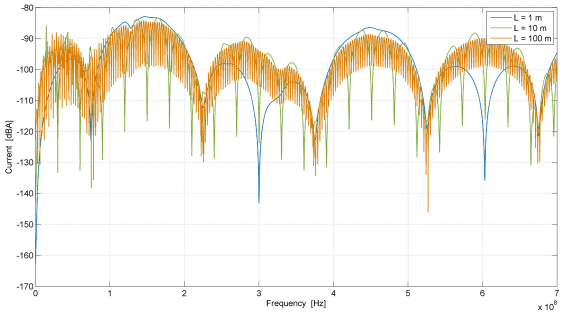

(b)

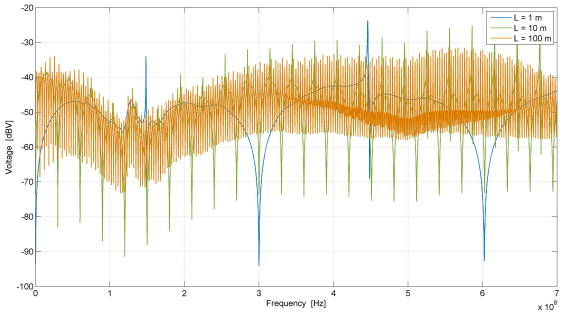

(c)

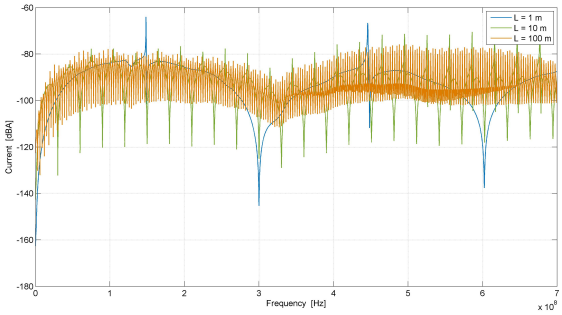

(d)

Figure 14. Induced voltage and current responses on the power port of PLC 3 as a function of frequency for various cable lengths and cable heights: (a) voltage, h = 1 m; (b) current, h = 1 m; (c) voltage, h = 1 cm; and (d) current, h = 1 cm.

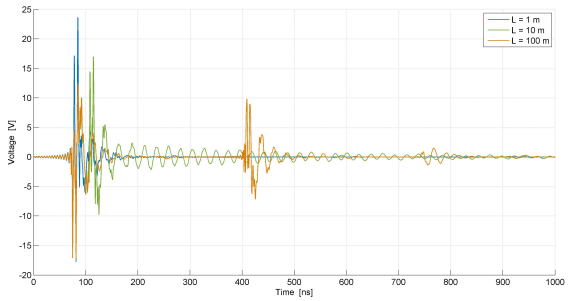

(a)

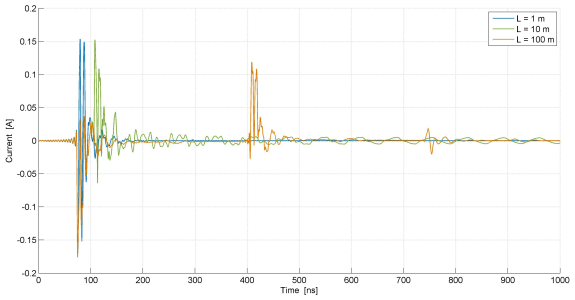

(b)

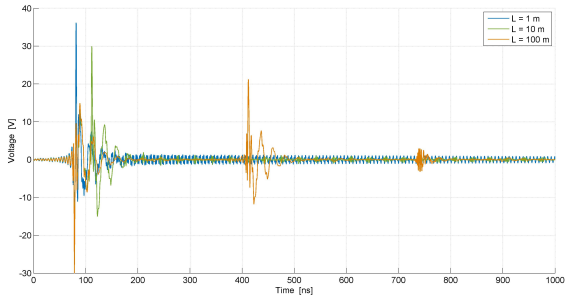

(c)

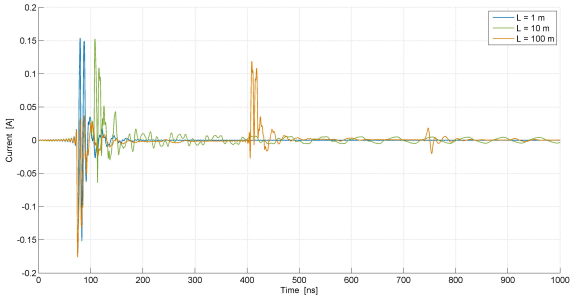

(d)

Figure 15. Induced voltage and current responses on the power port of PLC 1 as a function of time for various cable lengths and cable heights: (a) voltage, h = 1 m; (b) current, h = 1 m; (c) voltage, h = 1 cm; and (d) current, h = 1 cm.

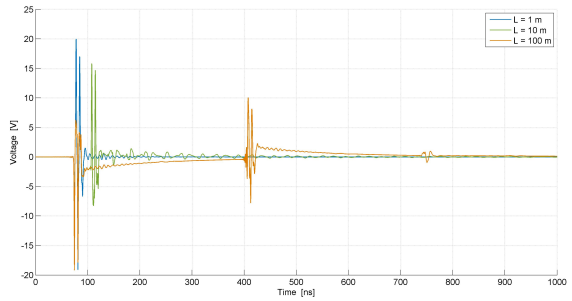

(a)

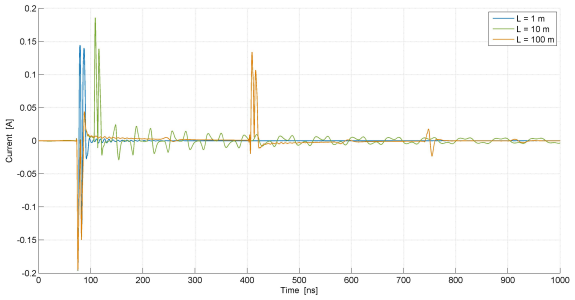

(b)

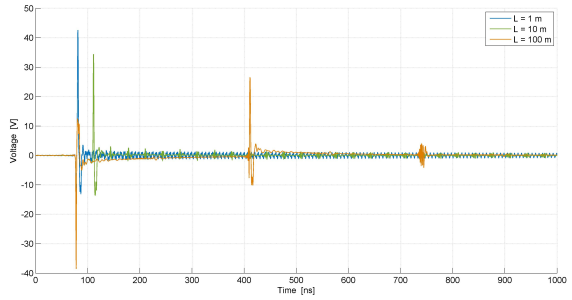

(c)

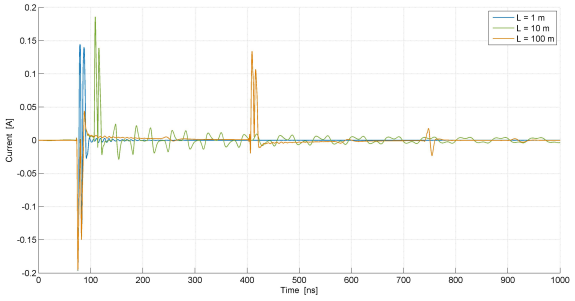

(d)

Figure 16. Induced voltage and current responses on the power port of PLC 2 as a function of time for various cable lengths and cable heights: (a) voltage, h = 1 m; (b) current, h = 1 m; (c) voltage, h = 1 cm; and (d) current, h = 1 cm.

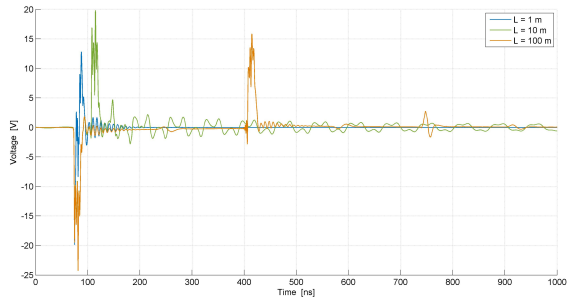

(a)

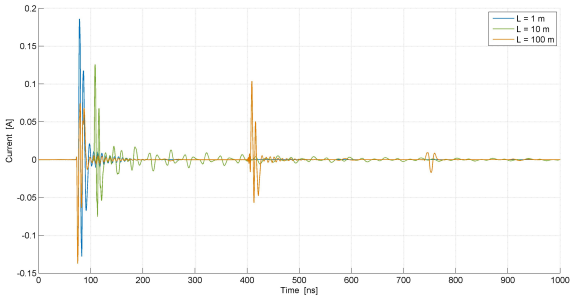

(b)

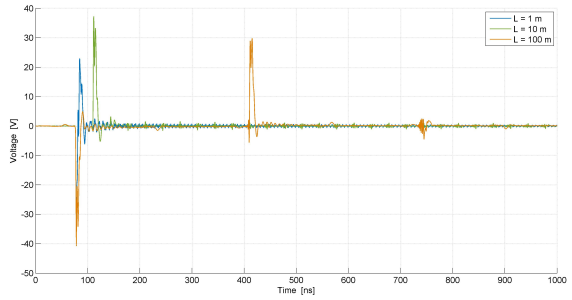

(c)

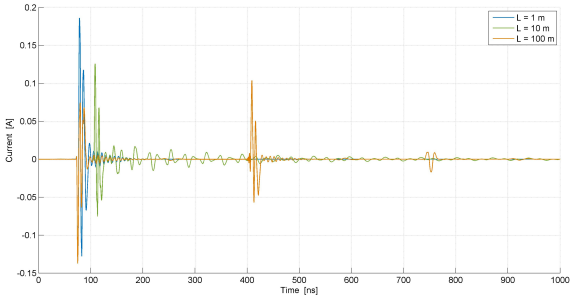

(d)

Figure 17. Induced voltage and current responses on the power port of PLC 3 as a function of time for various cable lengths and cable heights: (a) voltage, h = 1 m; (b) current, h = 1 m; (c) voltage, h = 1 cm; and (d) current, h = 1 cm.

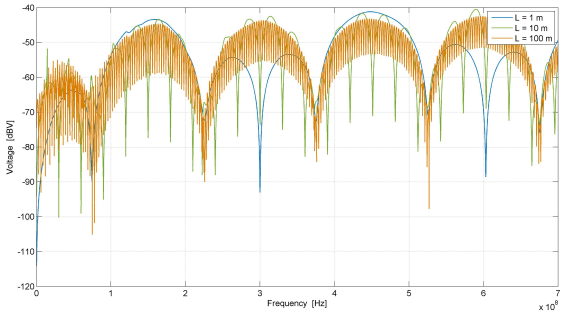

(a)

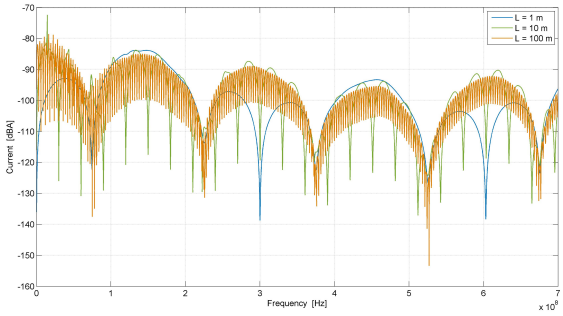

(b)

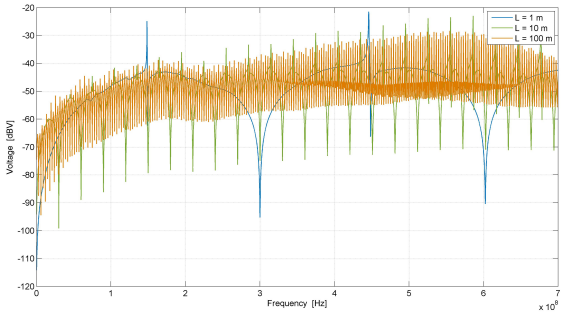

(c)

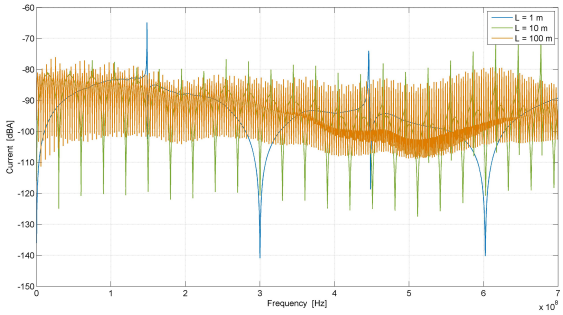

(d)

Figure 18. Induced voltage and current responses on the power port of the PMU (wire-wire) as a function of frequency for various cable lengths and cable heights: (a) voltage, h = 1 m; (b) current, h = 1 m; (c) voltage, h = 1 cm; and (d) current, h = 1 cm.

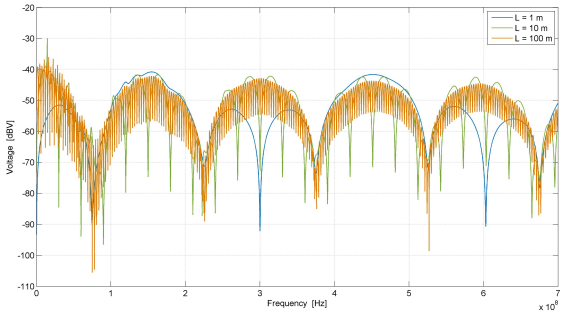

(a)

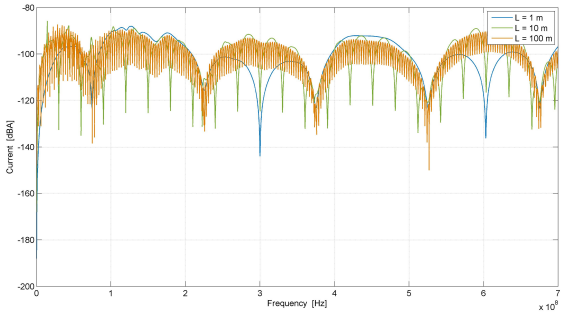

(b)

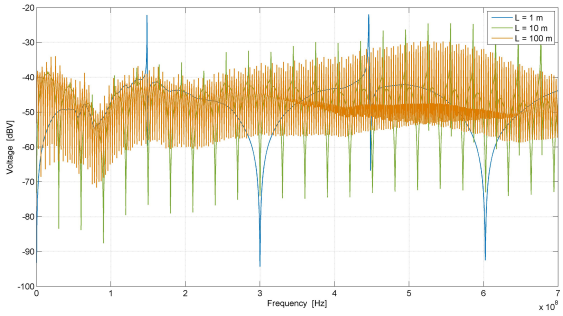

(c)

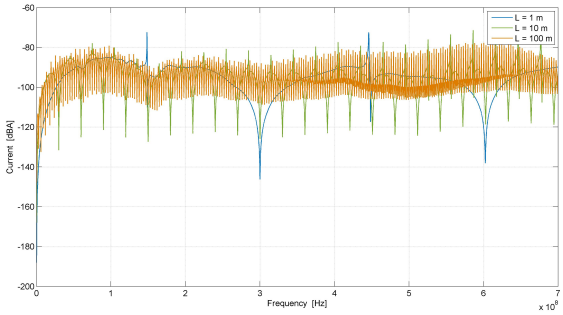

(d)

Figure 19. Induced voltage and current responses on the power port of the PMU (wire-ground) as a function of frequency for various cable lengths and cable heights: (a) voltage, h = 1 m; (b) current, h = 1 m; (c) voltage, h = 1 cm; and (d) current, h = 1 cm.

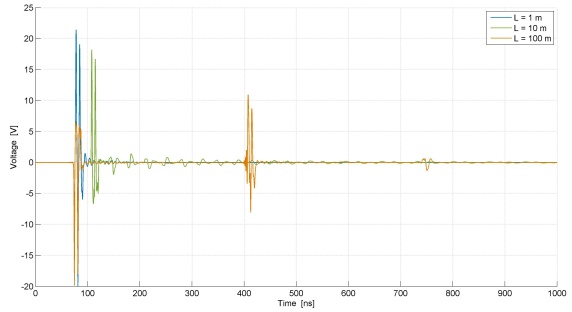

(a)

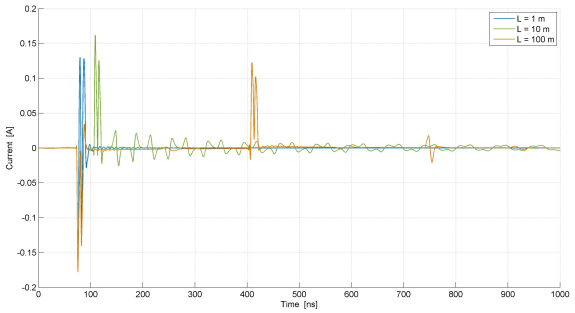

(b)

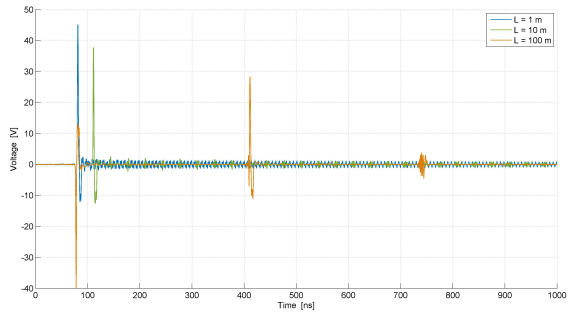

(c)

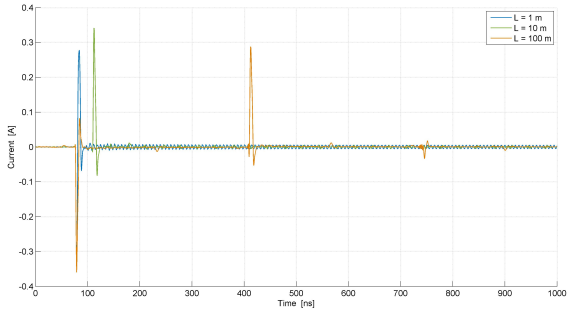

(d)

Figure 20. Induced voltage and current responses on the power port of the PMU (wire-wire) as a function of time for various cable lengths and cable heights: (a) voltage, h = 1 m; (b) current, h = 1 m; (c) voltage, h = 1 cm; and (d) current, h = 1 cm.

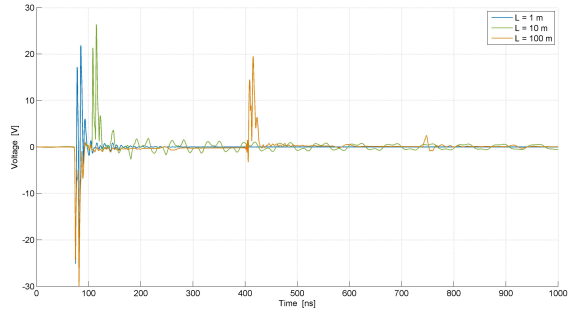

(a)

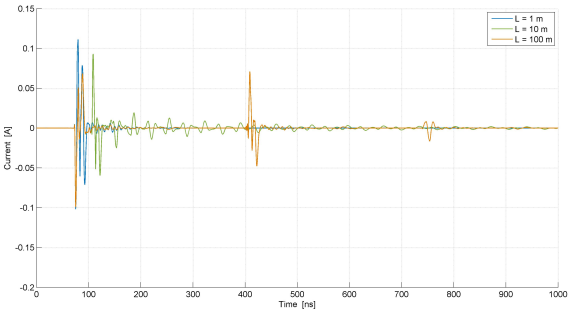

(b)

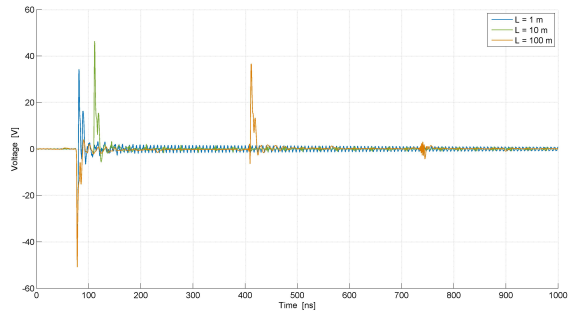

(c)

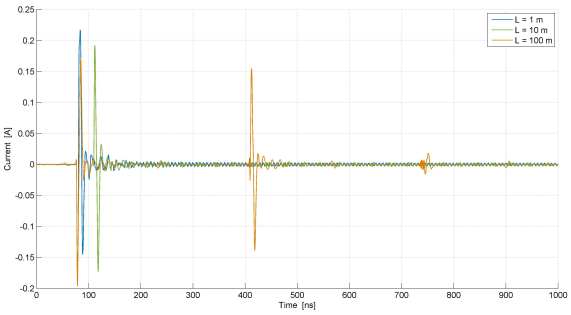

(d)

Figure 21. Induced voltage and current responses on the power port of the PMU (wire-ground) as a function of time for various cable lengths and cable heights: (a) voltage, h = 1 m; (b) current, h = 1 m; (c) voltage, h = 1 cm; and (d) current, h = 1 cm.

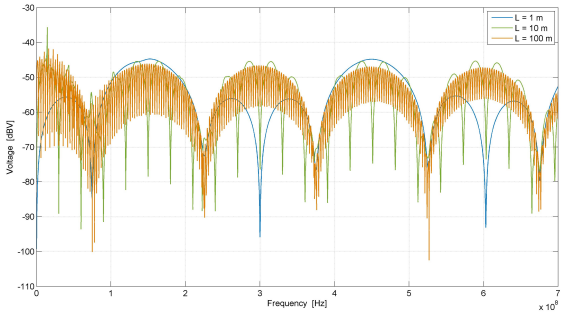

(a)

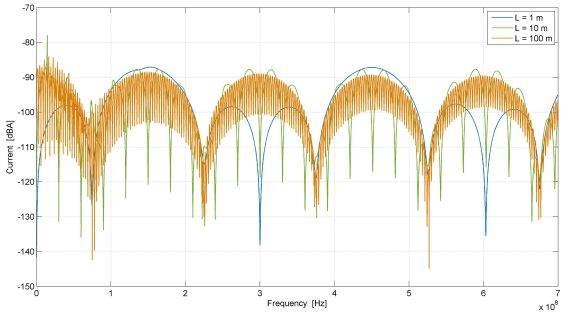

(b)

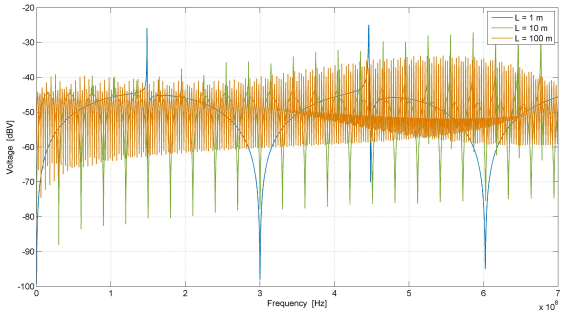

(c)

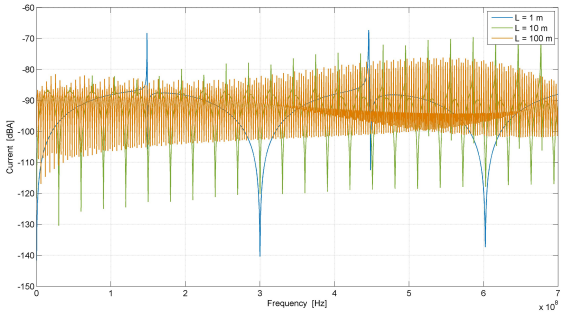

(d)

Figure 22. Induced voltage and current responses at the power port with matched loads as a function of frequency for various cable lengths and cable heights: (a) voltage, h = 1 m; (b) current, h = 1 m; (c) voltage, h = 1 cm; and (d) current, h = 1 cm.

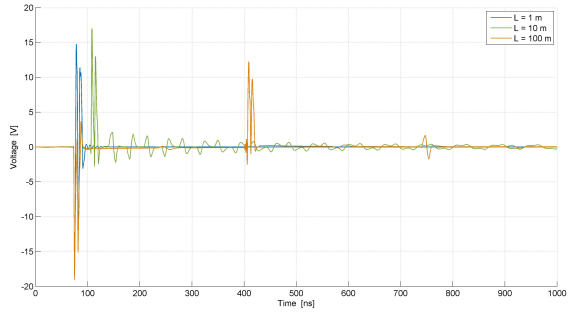

(a)

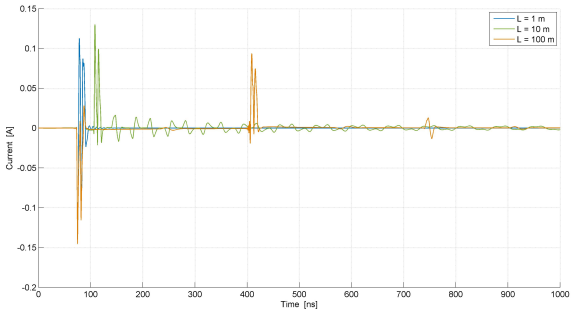

(b)

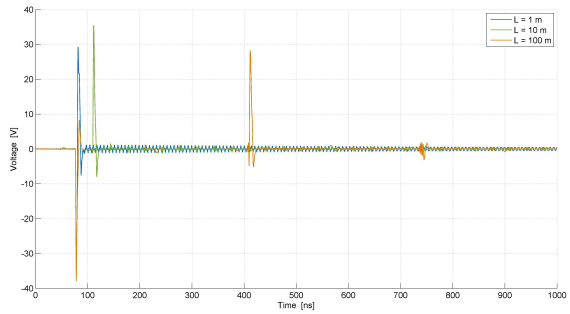

(c)

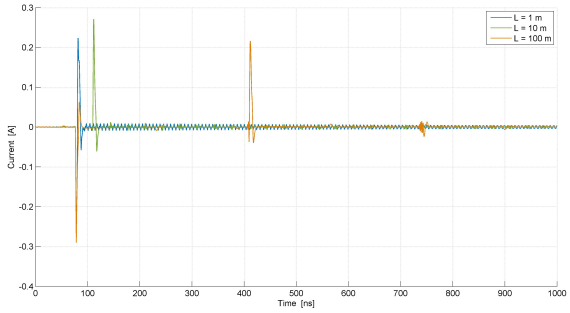

(d)

Figure 23. Induced voltage and current responses at the power port with matched loads as a function of time for various cable lengths and cable heights: (a) voltage, h = 1 m; (b) current, h = 1 m; (c) voltage, h = 1 cm; and (d) current, h = 1 cm.

Table 1. Peak voltages and currents induced at the equipment terminals

		PLC 1		PLC 2		PLC 3		PMU (wire-wire)		PMU (wire-ground)	
		$\|V_{pk}\|$ (V)	$\|I_{pk}\|$ (A)	$\|V_{pk}\|$ (V)	$\|I_{pk}\|$ (A)	$\|V_{pk}\|$ (V)	$\|I_{pk}\|$ (A)	$\|V_{pk}\|$ (V)	$\|I_{pk}\|$ (A)	$\|V_{pk}\|$ (V)	$\|I_{pk}\|$ (A)
L = 1 m	h = 1 cm	36.2	0.36	42.6	0.40	39.2	0.37	45.1	0.35	49.5	0.22
	h = 1 m	23.7	0.17	20.0	0.20	19.9	0.19	21.4	0.17	25.1	0.11
L = 10 m	h = 1 cm	30.0	0.36	38.4	0.39	40.6	0.27	40.0	0.36	50.7	0.20
	h = 1 m	17.0	0.18	19.0	0.20	24.1	0.14	19.8	0.18	29.9	0.10
L = 100 m	h = 1 cm	30.0	0.36	38.5	0.39	40.7	0.27	40.0	0.36	50.8	0.20
	h = 1 m	17.2	0.18	19.2	0.20	24.3	0.14	19.8	0.18	30.0	0.10

4. SUMMARY

As a follow-up study to a previous work on determining the shielding effectiveness of the facility building structure [6], this report presents a systematic approach to characterize the E1 HEMP-induced voltages and currents at the terminals of facility equipment connected to long cables and wires. The specific devices of interest included PLCs and PMUs, but the methods and techniques—which encompass a combination of practical measurement and simulation efforts—can be extended for the treatment and analysis of other electronic components and systems.

5. REFERENCES

[1] P. R. Barnes, B. W. McConnell, J. W. V. Dyke, F. M. Tesche, and E. F. Vance, "Electromagnetic pulse research on electric power systems: Program summary and recommendations," Tech. Rep. ORNL-6708, Oak Ridge National Laboratory, 1993.

[2] E. Savage, J. Gilbert, and W. Radasky, "The early-time (E1) high-altitude electromagnetic pulse (HEMP) and its impact on the U.S. power grid," Tech. Rep. Meta-R-320, 2010.

[3] C. Wilson, "High altitude electromagnetic pulse (HEMP) and high power microwave (HPM) devices: Threat assessments," tech. rep., Congressional Research Service, Library of Congress, Apr. 2006.

[4] D. Wang, Y. Li, P. Dehghanian, and S. Wang, "Power grid resilience to electromagnetic pulse (EMP) disturbances: A literature review," in *2019 North American Power Symposium (NAPS)*, 2019.

[5] R. Rashid and S. A. A. Gilani, "Electromagnetic pulse (EMP): A study of general trends, simulation analysis of E1 HEMP coupling and protection strategies," in *2021 International Conference on Cyber Warfare and Security (ICCWS)*, 2021.

[6] D. Liao, Z. Li, Y. Liu, L. Markel, B. McConnell, B. Poole, and L. Wang, "Estimation of high-altitude electromagnetic pulse signal leakage into power generation facilities: Simulations and measurements," Tech. Rep. ORNL/TM-2022/2779, Oak Ridge National Laboratory, 2022.

[7] E. B. Savage, J. L. Gilbert, and W. A. Radasky, "Expedient building shielding measurement method for HEMP assessments," *IEEE Transactions on Electromagnetic Compatibility*, vol. 55, no. 3, pp. 508–517, 2013.

[8] E. B. Savage, J. L. Gilbert, W. A. Radasky, and M. J. Madrid, "An alternative EM shielding effectiveness measurement method for buildings," in *2010 Asia-Pacific International Symposium on Electromagnetic Compatibility*, pp. 138–141, 2010.

[9] W. Qiu, L. Zhang, H. Yin, K. Sun, L. Markel, D. Liao, Z. Li, B. McConnell, and Y. Liu, "Port impedance measurement and current injection response analysis for PLCs," *IEEE Transactions on Industry Applications*, vol. 58, no. 6, pp. 7,838–7,846, 2022.

[10] L. Zhang, W. Qiu, H. Yin, K. Sun, L. Markel, D. Liao, Z. Li, B. McConnell, and Y. Liu, "Immunity study: Port impedance measurement of PMU and PCI testing under EMP," in *2022 IEEE/IAS Industrial and Commercial Power System Asia (ICPS Asia)*, 2022.

[11] Feko, "Altair feko," 2023. https://www.altair.com/feko/.

[12] C. Baum, T. Liu, and F. Tesche, "On the analysis of general multiconductor transmission line networks," Tech. Rep. Interaction Note 350, Kirtland Air Force Base, NM, 1978.

[13] C. E. Baum, "Generalization of the BLT equation," in *Proceedings of the 13th Zurich EMC Symposium*, 1999.

[14] F. Tesche, M. Ianoz, and T. Karlsson, *EMC Analysis Methods and Computational Models*. New York: John Wiley and Sons, 1997.

[15] F. M. Tesche, "Development and use of the BLT equation in the time domain as applied to a coaxial cable," *IEEE Transactions on Electromagnetic Compatibility*, vol. 49, no. 1, pp. 3–11, 2007.

[16] F. M. Tesche, J. M. Keen, and C. M. Butler, "Example of the use of the BLT equation for EM field propagation and coupling calculations," *URSI Radio Science Bulletin*, no. 312, pp. 32–47, 2005.

[17] F. Tesche and C. Butler, "On the addition of EM field propagation and coupling effects in the BLT equation," Tech. Rep. Interaction Note 588, Clemson University, Department of Electrical and Computer Engineering, 2004.